

Thermal Conductivity and Role of Phonon Scatterings in Suspended Thin Graphite Nanoribbons

Wonjae Jeon¹, Yu Pei¹, Renkun Chen^{1,*}

¹Department of Mechanical and Aerospace Engineering, University of California, San Diego, La
Jolla, California 92093, United States

*To whom correspondence should be addressed.

E-mail: rkchen@ucsd.edu

ABSTRACT

Thermal conductivity of thin graphitic materials has attracted significant interests due to their applications in thermal management such as fillers in polymer composites for thermal interface materials and heat exchangers. Recently graphite nanoribbons have also been under investigations for intriguing phonon hydrodynamic transport. However, graphite ribbons with thickness in the range of hundreds of nanometers have not been measured despite their importance as both thermal conductivity fillers and as a testbed for phonon hydrodynamics. In this work, we developed a process to exfoliate graphite nanoribbons within this thickness range and with length up to 1 mm and transferred them to a suspended platform to measure their thermal conductivity. We obtained thermal conductivity around 800 W/m-K at room temperature. With decreasing temperature, the thermal conductivity initially increased and peaked at around 150 K, with peak

values ranging from 1000 to 1600 W/m-K for ribbon thickness of 352 to 680 nm. This temperature dependence suggests the strong phonon *Umklapp* scattering, which is consistent with the absence of the phonon hydrodynamics observed in our experiments, as shown by nearly identical thermal conductivity in two samples with similar thickness (525 and 560 nm) and different lengths (0.5 and 1 mm). This is contrary to the previous experimental results suggesting phonon hydrodynamic at room temperature on even thicker ribbons. Finally, the lower than bulk value of thermal conductivity reveals strong phonon boundary scattering, suggesting long phonon mean free path, on the order of 100s nm, in the cross-plane direction of graphite, confirming certain previous studies.

KEYWORDS

Thin graphite, thermal conductivity, thickness-dependent measurement, phonon mean free path

INTRODUCTION

Advancements in high-power portable electronic devices and their miniaturization have led to an increased demand for enhanced thermal management to manage the rising specific heat flux.^{1,2} To meet this demand, materials having high thermal conductivity (κ) and lightweight are increasingly demanded. Graphene has received considerable attention due to its high in-plane κ (5300 W m⁻¹ K⁻¹) at room temperature, which is attributed to its strong covalent bonding^{3,4} It has shed light on the heat dissipation application in nanoelectronics. Few-layer graphene has been utilized as a heat spreader in high-power gallium nitride (GaN) transistor.⁵ However, the graphene has a limited heat dissipation rate owing to its atomically thin structure, therefore, a larger number of graphene layers is required to be utilized in the cooling of high-power microdevices.⁶ Bulk

highly ordered pyrolytic graphite (HOPG) has a far higher in-plane κ ($1950 \text{ W m}^{-1} \text{ K}^{-1}$)⁷ than metals such as aluminum ($\sim 237 \text{ W m}^{-1} \text{ K}^{-1}$) and copper ($\sim 401 \text{ W m}^{-1} \text{ K}^{-1}$) at room temperature.⁸ As a result, graphite has been extensively studied in various heat dissipation systems, including heat sinks, thermal interface materials, and heat spreaders.⁹⁻¹² However, the discrepancy in κ between graphene and graphite has not been fully explored.

In order to better understand thermal transport mechanisms at different sizes, it is important to conduct size-dependent investigations. For instance, investigating the quantization effect by varying the diameter of nanowires can be a useful approach, as demonstrated by the study of NbSe₃ nanowires.¹³ During the diameter of NbSe₃ nanowires decreases from 135 nm to 26 nm, the κ decreases from 7.1 to 4.3 $\text{W m}^{-1} \text{ K}^{-1}$ due to the confinement effect, which induced increased boundary scattering of three-dimensional (3D) phonons at the nanowire surfaces.¹³ However, as the diameter decreased further from 26 nm to 6.8 nm, the κ started to increase, reaching 109 $\text{W m}^{-1} \text{ K}^{-1}$ as a result of the excitation of one-dimensional (1D) phonons.¹³ To investigate the heat transport phenomena between graphene and graphite, which are two-dimensional (2D) materials, a thickness-dependent thermal transport investigation is needed.

Recently, phonon hydrodynamics in thin graphite (TG) with a few micrometer thickness has been reported, showing an extremely high κ of 4300 $\text{W m}^{-1} \text{ K}^{-1}$ in 8.5 μm thick graphite at room temperature, as measured by a thermocouple method.¹⁴ The paper suggests that the occurrence of phonon hydrodynamics in thin graphite is attributed to a decrease in the relative weight of Umklapp (U) scattering, which causes phonons to lose momentum during collisions.¹⁴ This effect becomes more pronounced as the graphite thickness is reduced, leading to a higher κ .¹⁴ In contrast, Li *et al.* reported the opposite trend of κ based on Monte Carlo (MC) calculation

showing a decreasing κ with the decreased thickness from 65 μm to several nanometers.¹⁵ They measured κ of TG between 4.4 to 7.7 nm thicknesses using a four-probe method and their result matched well with the MC calculation.¹⁵ However, phonon hydrodynamics was not observed due to the small sample dimensions (width is 1.75 μm and thickness is < 7.7 nm) compared to the mean free path (MFP) of momentum-conserving normal (N) scattering along the in-plane and cross-plane direction of TG.¹⁵ These contrasting results have motivated us to re-investigate the thermal transport in TG.

Here we present the experimentally measured κ of TG less than 1 μm thicknesses. Mechanically exfoliated graphite flakes having 352 – 680 nm thicknesses were etched into ribbons of >0.5 mm lengths and ~ 110 μm widths. They were then transferred onto microdevices designed for κ measurement using a four-probe 3ω measurement technique. The suspended length of TG ribbons between the heater/thermometer pad and heat sink are 0.5 and 1 mm, resulting in aspect ratios of length to width of 5 and 10, respectively. The measured κ of TG in the temperature regime from 50 to 360 K lies between those of 2.45 nm thickness TG and bulk HOPG.^{7, 15} At 100 K, the κ increases from 958 to 1623 $\text{W m}^{-1} \text{K}^{-1}$ as the thickness increases from 352 to 680 nm, showing the thickness-dependence of κ in TG. We also observed the decreasing peak temperature as the graphite thickness increased.

RESULTS AND DISCUSSION

Thin graphite ribbon preparation and its transfer to the device.

To investigate the thermal transport in TGs with thicknesses in the hundreds of nanometers, we exfoliated HOPG using an improved tape method to obtain residue-free TG flakes (see the

details in Supplementary Note S1 and Figure S1). The flakes were then etched into ribbons using oxygen plasma etching with a shadow mask. Next, a TG ribbon was transferred to a microfabricated device for κ measurement, as shown in a schematic drawing and scanning electron microscopy (SEM) image of Figure 1a, b. Details of device fabrication processes and TG transfer are provided in Supplementary Note S2 and Figures S2 and S3. The suspended membrane, where one end of the TG is placed, consists of an integrated Pt coil between the top and bottom Al_2O_3 layers (see inset in Figure 1a). The Pt coil acts as a heater/resistance-thermometer, generating heat via Joule heating and measuring temperature rise using the temperature coefficient of resistance (TCR). The details of the κ measurement will be discussed later. An additional Pt film was deposited on the top Al_2O_3 insulation layer not only to reduce the thermal contact resistance by increasing the surface energy with graphite/metal contact rather than graphite/oxide contact,^{16, 17} but also to obtain a uniform temperature profile on the membrane. Furthermore, a drop-dry method using isopropyl alcohol (IPA) was introduced to enhance the van der Waals forces between the graphite and the device interfaces.^{18, 19} The suspended length of the TG ribbon (L_{TG}) is determined by the distance between the heater/thermometer membrane and the heat sink. The width of the ribbon is measured using an optical microscope and the thickness is obtained by scanning the ribbon surface placed on the heat sink using a surface profilometer. To verify the uniform thickness of the TG ribbon, an area-scanning of TG ribbon on the heat sink area was conducted and its 3D map is shown in Supplementary Figure S4, showing high uniformity. We also scanned another TG ribbon that was transferred from the same TG flake to a bare Si wafer using the same transfer method and confirmed that the thicknesses of the ribbons from the same flake are almost identical with high uniformity, not only along a single ribbon. SEM images and surface profiles of TG ribbons measured in this work are presented in Supplementary Figure S5 - S8. The dimensions of

TG samples are listed in Table 1.

Thermal conductivity measurement of thin graphite.

Figure 1c shows a circuit diagram for the four-probe 3ω method, which we used to measure the κ of the TG. The measurements were carried out under a vacuum pressure of $\sim 4.5 \times 10^{-5}$ torr. The temperature rise of the heater/thermometer membrane ($\Delta T_h = T_h - T_0$) from the ambient temperature (T_0) was directly obtained from the resistance change of the heater/thermometer (ΔR_h) and converted to ΔT_h based on the TCR ($\frac{dR_h}{dT}$), following previously published protocols.²⁰⁻²² The generated heat flux from the heater ($Q_t = Q_{TG} + Q_b$) conducts through both TG (Q_{TG}) and bridge beams (Q_b). With the measured ΔT_h and Q_t , the combined thermal conductance ($G_t = G_{TG} + G_b = \frac{Q_t}{\Delta T_h}$) of TG (G_{TG}) and beams (G_b) can be calculated (Supplementary Figure S9).²⁰⁻²² To evaluate the effective G_{TG} , we measured the G_b with a reference sample that was fabricated from the same batch and doesn't have the TG. The reference sample's heater/thermometer membrane has an almost identical structure and dimension and was heated up with the same heating power condition as the device with the TG ribbon. Since the reference sample doesn't have the TG, the generated heat flux only conducts through the suspended beams. As a result, $G_b (= \frac{Q_b}{\Delta T_{h,ref}})$ can be calculated based on the temperature rise of the reference device's heater/thermometer membrane ($\Delta T_{h,ref}$). Finally, G_{TG} was obtained by subtracting G_b from G_t , and the κ of TG was obtained by $\kappa = \frac{G_{TG} \cdot L_{TG}}{A_{TG}}$, where A_{TG} is the cross-sectional area of the TG ribbon.

To verify the reliability of our method for measuring κ , the κ of Pt ribbon having 2 μm width, 110 nm thickness, and 200 μm length was measured (Supplementary Figure S10). The measured κ using our electrothermal system was $41.6 \text{ W m}^{-1} \text{ K}^{-1}$ at 300 K. The measured κ value

was compared to the estimated value calculated from electrical conductivity (σ) using the Wiedemann-Franz law ($\frac{\kappa}{\sigma} = LT$, where L is the Lorenz number ($2.44 \times 10^{-8} \text{ V}^2 \text{ K}^{-2}$) and T is the temperature).²³ This comparison was made because most of the heat transport in metals originates from free electrons. The estimated κ was $40.1 \text{ W m}^{-1} \text{ K}^{-1}$, showing approximately 4% lower than the measured value. This discrepancy may be attributed to the contribution of lattice thermal effects to the total κ value. Despite this difference, the results support that our measurement method used is reliable.

Figure 2a shows the temperature dependence of κ for TGs between 50 K to 360 K. The error bars depict the combined uncertainties from multiple measured data points for G_{TG} and the characterization of TG ribbons' dimension, which are less than ~4%. (see the detail in Supplementary Note S3).²⁰⁻²² At temperatures below ~150 K, κ decreases as temperature decreases because the c-axis MFP increases at lower temperatures, resulting in increased phonon boundary scattering. The c-axis MFP was estimated to reach up to 600 nm at around 40 K.²⁴ For a thickness of 680 nm, the measured κ at 50 K ($\sim 1100 \text{ W m}^{-1} \text{ K}^{-1}$) is much larger than that of thinner samples (352 – 560 nm, $500 - 580 \text{ W m}^{-1} \text{ K}^{-1}$). This could be the experimental evidence of c-axis MFP at low temperatures (~600 nm) where boundary scattering barely occurs in 680 nm thick graphite, while it is dominant in 352 – 560 nm thicknesses where the c-axis MFP is longer than their thicknesses. Above 150 K, the c-axis MFP keeps decreasing with increasing temperature as various phonon momentum-losing processes, such as Umklapp, inelastic, and impurity scattering, become more active.^{24,25} Figure 2b shows the relationship between κ and thickness at various temperatures. At 50, 100, and 200 K, κ increases as the thickness increases. However, at room temperature, the measured κ for different thicknesses are similar in the range of $860 - 920 \text{ W m}^{-1} \text{ K}^{-1}$. This could

be due to the smaller c-axis MFP (100 – 200 nm)^{24, 25} than their thicknesses at 300 K, inducing prevalent momentum-losing scatterings from defects or grain boundaries.

Phonon hydrodynamics with extremely high κ as of 4300 W m⁻¹ K⁻¹ at room temperature has been reported in 8.5 μ m thick HOPG, which was measured by a thermocouple method.¹⁴ It has also been suggested that thinner graphite than 8.5 μ m can have even higher κ than 4300 W m⁻¹ K⁻¹.¹⁴ To investigate whether phonon hydrodynamics can occur in our measured range of 352 – 680 nm thickness of TGs, we analyzed the exponent of the temperature dependence of κ (α), which is defined as $\alpha = \frac{d(\ln \kappa)}{d(\ln T)}$, as shown in Figure 2c. The dashed line represents the ballistic limit of phonon transport, and it has been reported that when α exceeds the ballistic limit, where a faster increase in κ than the ballistic limit is observed, it could be strong evidence of the occurrence of phonon hydrodynamics.^{14, 15, 26-29} Our measurements for the 352 – 680 nm thickness TGs show a value of α less than 1.5, resulting in no occurrence of Phonon Poiseuille flow. This could be due to the up to a few μ m long MFP of N-scattering in the c-axis at low temperatures.¹⁵ Additionally, the high concentration of ¹³C isotope in natural graphite (~1.1% in HOPG) induces resistive phonon-isotope scattering, which is a momentum-destroying process, restricting the occurrence of phonon hydrodynamics.^{26, 28, 29}

The κ of TGs with thicknesses ranging from 352 to 680 nm was compared with other different thicknesses of HOPGs, including those from 2.45 nm to 1 mm (bulk HOPG) (Figure 3a).^{7, 14, 15, 30} The measured κ of 352 to 680 nm thickness was found to be larger than that of 2.45 and 7.7 nm thick exfoliated HOPG, where the momentum-losing boundary scattering dominates due to the thickness being smaller than the c-axis phonon MFP,^{24, 25} while it was smaller than that of bulk HOPG with a thickness of 1 mm, indicating a thickness-dependence of κ . This trend is

consistent with MC simulations, which show a higher κ as the thickness increases from several nanometers to 65 μm .¹⁵ In contrast, the κ measured by the thermocouple method decreases as the thickness increases from 8.5 to 580 μm , exhibiting the opposite trend.¹⁴ At temperatures above 150 K, the κ of 8.5 μm thick graphite is even higher than that of bulk HOPG, reaching up to 4300 $\text{W m}^{-1} \text{K}^{-1}$ at room temperature. This could be attributed to the long N-scattering phonon MFP, which is comparable to the 8.5 μm thickness at low temperature (50 K), where phonon Poiseuille flow can occur.¹⁵ However, at room temperature, the N-scattering MFP is significantly smaller than the micrometer scale, as thus phonon hydrodynamics is barely present.¹⁵ Moreover, the presence of the isotopes in the natural graphite ($\sim 1.1\%$ ^{13}C in HOPG) can hinder phonon hydrodynamics due to resistive phonon-isotope scattering, which is a momentum-destroying process.^{26, 28, 29} Therefore, further studies in a similar thickness scale and the isotope effect of TG are needed to interpret the ultra-high κ of 8.5 μm thick HOPG, which exceeds that of bulk HOPG.

Figure 3b shows the κ peak temperatures of different thicknesses of HOPG.^{7, 14, 15, 30} The results of this work show that the peak temperature decreases from 181.7 K to 137.3 K as the thickness increases from 352 nm to 680 nm. These peak temperatures are smaller than those of 2.45 nm (292 K) and 7.7 nm (286 K) thick HOPG, while larger than that of the bulk HOPG (1 mm thick) (118 K), indicating a clear dependence of the peak temperature on thickness.^{7, 15, 30} The κ of HOPGs with thicknesses of 8.5, 240, and 580 μm , measured using the thermocouple method, also decreases as the thickness increases, although the peak temperature range overlaps with our measurement results. Further experimental investigation in a similar thickness range is required to fully understand the thickness-dependence of the peak temperature.¹⁵

In conclusion, this study investigated the thermal transport in suspended TG ribbons in

352 – 680 nm thicknesses four-probe 3ω method. The TGs were mechanically exfoliated and suspended on the microfabricated device. The experimentally measured κ of TGs in the temperature range from 50 to 360 K lies between those of 2.45 nm thickness TG and bulk HOPG. The results show that the κ of HOPGs increase with the thickness as predicted by the MC simulation,¹⁵ while the peak temperature decreases as the graphite thickness increases. Phonon hydrodynamics doesn't occur in this thickness range at low temperatures which is possibly due to momentum-losing scatterings such as boundary scattering (thinner than c-axis N-scattering MFP) and phonon-isotope scattering ($\sim 1.1\%$ ^{13}C in HOPG).^{24-26, 28, 29} These findings provide insights into the thickness-dependent thermal transport in TG, which is important for the development of high-performance heat dissipation systems for microdevices. Further studies are needed to elucidate the mechanisms responsible for the thickness-dependent in κ TGs.

ASSOCIATED CONTENT

Supporting Information

The Supporting Information is available free of charge on the ACS Publications website at DOI: xxx.

- Thin graphite ribbon preparation; device fabrication and graphite ribbon transfer; uniformity of graphite ribbon thickness; SEM images and surface profiles of thin graphite ribbons; uncertainty analysis; heating power dependent temperature rise of heater/thermometer membrane with and without graphite ribbon; optical image of Pt ribbon device.

AUTHOR INFORMATION

Corresponding Author

*E-mail: rkchen@ucsd.edu.

ORCID

Renkun Chen: 0000-0001-7526-4981

Author Contributions

W.J. and P.Y. carried out the experiments. W.J., P.Y., and R.C. designed the experiments. W.J. and R.C. conceived the research idea, interpreted the results, and wrote the manuscript.

Notes

The authors declare no competing financial interest.

REFERENCES

- (1) Fu, Y.; Nabiollahi, N.; Wang, T.; Wang, S.; Hu, Z.; Carlberg, B.; Zhang, Y.; Wang, X.; Liu, J. A complete carbon-nanotube-based on-chip cooling solution with very high heat dissipation capacity. *Nanotechnology* **2012**, *23* (4), 045304. DOI: 10.1088/0957-4484/23/4/045304.
- (2) Kwon, B.; Foulkes, T.; Yang, T.; Miljkovic, N.; King, W. P. Air jet impingement cooling of electronic devices using additively manufactured nozzles. *IEEE Transactions on Components, Packaging and Manufacturing Technology* **2019**, *10* (2), 220-229.
- (3) Slack, G. A. Nonmetallic crystals with high thermal conductivity. *Journal of Physics and Chemistry of Solids* **1973**, *34* (2), 321-335. DOI: [https://doi.org/10.1016/0022-3697\(73\)90092-9](https://doi.org/10.1016/0022-3697(73)90092-9).

- (4) Balandin, A. A.; Ghosh, S.; Bao, W.; Calizo, I.; Teweldebrhan, D.; Miao, F.; Lau, C. N. Superior Thermal Conductivity of Single-Layer Graphene. *Nano letters* **2008**, *8* (3), 902-907. DOI: 10.1021/nl0731872.
- (5) Yan, Z.; Liu, G.; Khan, J. M.; Balandin, A. A. Graphene quilts for thermal management of high-power GaN transistors. *Nature communications* **2012**, *3* (1), 827. DOI: 10.1038/ncomms1828.
- (6) Subrina, S.; Kotchetkov, D.; Balandin, A. A. Graphene heat spreaders for thermal management of nanoelectronic circuits. *arXiv preprint arXiv:0910.1883* **2009**.
- (7) Touloukian, Y. S.; Powell, R.; Ho, C.; Klemens, P. *Thermophysical properties of matter-the tprc data series. volume 2. thermal conductivity-nonmetallic solids.(reannouncement). data book*; Purdue Univ., Lafayette, IN (United States). Thermophysical and Electronic ..., 1971.
- (8) Incropera, F. P.; Lavine, A. S.; Bergman, T. L.; DeWitt, D. P. *Principles of heat and mass transfer*; Wiley, 2013.
- (9) Fan, W.; Liu, X. Advancement in high thermal conductive graphite for microelectronic packaging. In *RF and Microwave Microelectronics Packaging II*, Springer, 2017; pp 129-145.
- (10) Cermak, M.; Kenna, J.; Bahrami, M. Natural-graphite-sheet based heat sinks. In *2017 33rd Thermal Measurement, Modeling & Management Symposium (SEMI-THERM)*, 2017; IEEE: pp 310-313.
- (11) Zhou, J.; Fan, X.; Zhu, J.; Zhang, Z.; Tang, D. Systematic Investigations on the Thermal Management Performance of Graphite Thin Films for High-Electron-Mobility Transistors. *IEEE Transactions on Electron Devices* **2022**, *69* (12), 6637-6643.
- (12) Tian, X.; Itkis, M. E.; Bekyarova, E. B.; Haddon, R. C. Anisotropic thermal and electrical properties of thin thermal interface layers of graphite nanoplatelet-based composites. *Sci Rep-Uk* **2013**, *3* (1), 1-6.

- (13) Yang, L.; Tao, Y.; Zhu, Y.; Akter, M.; Wang, K.; Pan, Z.; Zhao, Y.; Zhang, Q.; Xu, Y.-Q.; Chen, R.; et al. Observation of superdiffusive phonon transport in aligned atomic chains. *Nature nanotechnology* **2021**, *16* (7), 764-768. DOI: 10.1038/s41565-021-00884-6.
- (14) Machida, Y.; Matsumoto, N.; Isono, T.; Behnia, K. Phonon hydrodynamics and ultrahigh-temperature thermal conductivity in thin graphite. *Science* **2020**, *367* (6475), 309-+. DOI: 10.1126/science.aaz8043.
- (15) Li, X.; Lee, H. J.; Ou, E. R.; Lee, S. Y.; Shi, L. Reexamination of hydrodynamic phonon transport in thin graphite. *J Appl Phys* **2022**, *131* (7). DOI: Artn 075104
10.1063/5.0078772.
- (16) Blonski, S.; Garofalini, S. H. Molecular dynamics simulations of α -alumina and γ -alumina surfaces. *Surface Science* **1993**, *295* (1), 263-274. DOI: [https://doi.org/10.1016/0039-6028\(93\)90202-U](https://doi.org/10.1016/0039-6028(93)90202-U).
- (17) Vitos, L.; Ruban, A. V.; Skriver, H. L.; Kollár, J. The surface energy of metals. *Surface Science* **1998**, *411* (1), 186-202. DOI: [https://doi.org/10.1016/S0039-6028\(98\)00363-X](https://doi.org/10.1016/S0039-6028(98)00363-X).
- (18) Kim, J.; Seo, D.-J.; Park, H.; Kim, H.; Choi, H.-J.; Kim, W. Extension of the T-bridge method for measuring the thermal conductivity of two-dimensional materials. *Review of Scientific Instruments* **2017**, *88* (5), 054902.
- (19) Shin, S.; Chen, R. Thermal transport measurements of nanostructures using suspended micro-devices. In *Nanoscale Energy Transport*; IOP Publishing, 2020; pp 12-11-12-33. DOI: 10.1088/978-0-7503-1738-2ch12.
- (20) Shin, S.; Elzouka, M.; Prasher, R.; Chen, R. Far-field coherent thermal emission from polaritonic resonance in individual anisotropic nanoribbons. *Nature communications* **2019**, *10* (1), 1377. DOI: 10.1038/s41467-019-09378-5.

- (21) Shin, S. M.; Chen, R. K. Plasmonically Enhanced Thermal Radiation by Means of Surface Phonon Polaritons. *Phys Rev Appl* **2020**, *14* (6). DOI: ARTN 064013
10.1103/PhysRevApplied.14.064013.
- (22) Wingert, M. C.; Chen, Z. C. Y.; Dechaumphai, E.; Moon, J.; Kim, J.-H.; Xiang, J.; Chen, R. Thermal Conductivity of Ge and Ge–Si Core–Shell Nanowires in the Phonon Confinement Regime. *Nano letters* **2011**, *11* (12), 5507-5513. DOI: 10.1021/nl203356h.
- (23) Cheng, Z.; Liu, L.; Xu, S.; Lu, M.; Wang, X. Temperature dependence of electrical and thermal conduction in single silver nanowire. *Sci Rep-Uk* **2015**, *5* (1), 1-12.
- (24) Zhang, H.; Chen, X.; Jho, Y.-D.; Minnich, A. J. Temperature-Dependent Mean Free Path Spectra of Thermal Phonons Along the c-Axis of Graphite. *Nano letters* **2016**, *16* (3), 1643-1649. DOI: 10.1021/acs.nanolett.5b04499.
- (25) Fu, Q.; Yang, J.; Chen, Y.; Li, D.; Xu, D. Experimental evidence of very long intrinsic phonon mean free path along the c-axis of graphite. *Applied Physics Letters* **2015**, *106* (3), 031905. DOI: 10.1063/1.4906348.
- (26) Huang, X.; Guo, Y.; Wu, Y.; Masubuchi, S.; Watanabe, K.; Taniguchi, T.; Zhang, Z.; Volz, S.; Machida, T.; Nomura, M. Observation of phonon Poiseuille flow in isotopically-purified graphite ribbons. *arXiv preprint arXiv:2207.01469* **2022**.
- (27) Li, X.; Lee, S. Role of hydrodynamic viscosity on phonon transport in suspended graphene. *Phys Rev B* **2018**, *97* (9), 094309.
- (28) Cepellotti, A.; Fugallo, G.; Paulatto, L.; Lazzeri, M.; Mauri, F.; Marzari, N. Phonon hydrodynamics in two-dimensional materials. *Nature communications* **2015**, *6* (1), 6400.
- (29) Lee, S.; Broido, D.; Esfarjani, K.; Chen, G. Hydrodynamic phonon transport in suspended graphene. *Nature communications* **2015**, *6* (1), 6290.

(30) Ou, E.; Li, X.; Lee, S.; Watanabe, K.; Taniguchi, T.; Shi, L. Four-Probe Measurement of Thermal Transport in Suspended Few-Layer Graphene With Polymer Residue. *J Heat Trans-T Asme* **2019**, *141* (6). DOI: Artn 061601

10.1115/1.4043167.

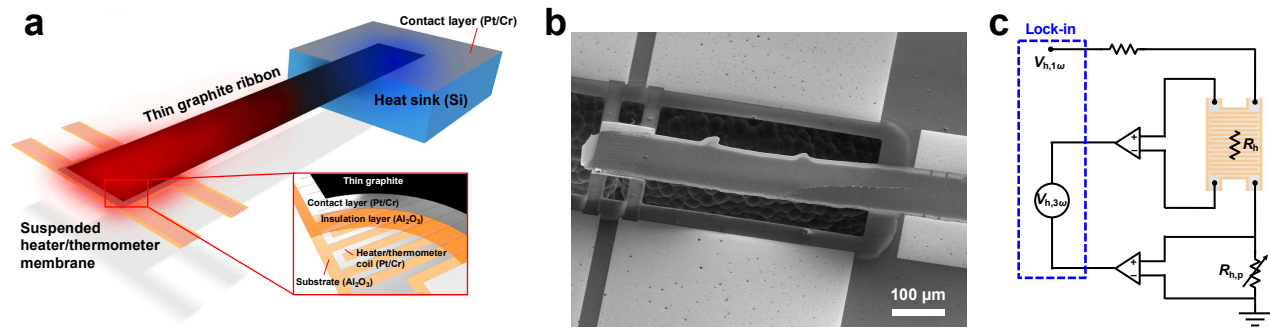


Figure 1. Device for thermal conductivity measurement of thin graphite ribbon. (a) Schematic illustration and (b) SEM image of the device showing the suspended thin graphite ribbon between the suspended heater/thermometer and the heat sink. The specific structure of the heater/thermometer is shown in the inset of figure (a). The corresponding sample of SEM image is ~ 560 nm thick graphite ribbon (sample ID: TG3). (c) Diagram of AC modulated heating of four-probe 3ω measurement system, where the heater is heated by a 1ω current through the longest path of the heating coil, and the corresponding resistance change (ΔR_h) due to the temperature rise is measured from the 3ω voltage through the shortest path of the heating coil.

Table 1. Summary of dimensions of measured thin graphite ribbons.

Samples	Thickness (nm)	Width (μm)	Length (mm)
TG1	352	96	1
TG2	525	113	1
TG3	560	118	0.5
TG4	680	116	0.5

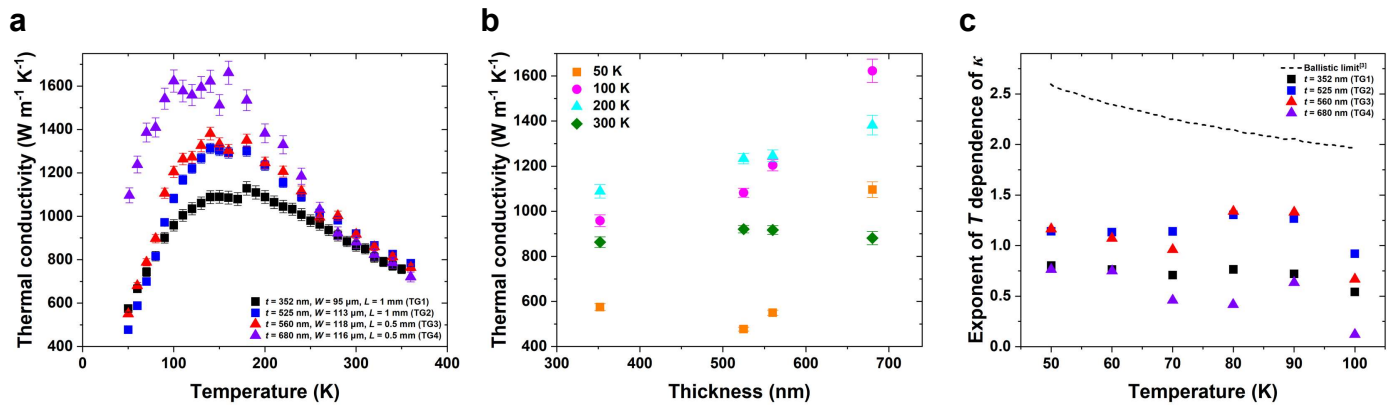


Figure 2. Thermal transport properties of measured thin graphite ribbons. (a) Temperature dependence of thermal conductivity of thin graphite ribbons. (b) Thickness dependence of thermal conductivity of thin graphite ribbons at temperatures 50, 100, 200, and 300 K. Error bars for figures (a) and (b) indicate uncertainties from thermal conductance measurements and thin graphite ribbon dimension characterization. (c) Exponent of temperature dependence of thermal conductivity for measured thin graphite ribbons is compared with the ballistic limit at 50 – 100 K. ^[ref]

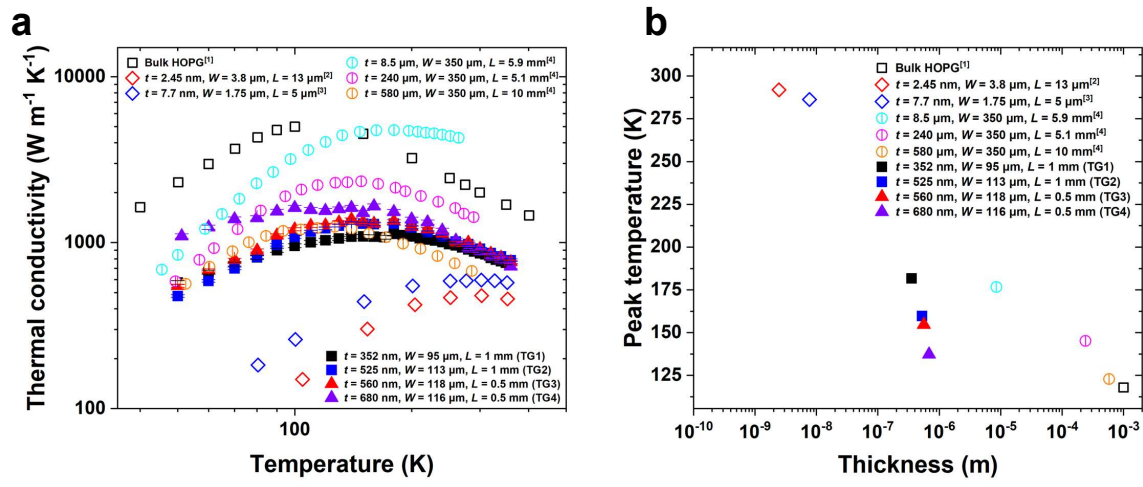


Figure 3. Comparison of thermal transport properties of thin graphite ribbons (a) Comparison of the thermal conductivity results for the measured thin graphite ribbons (352 – 680 nm thickness) with reported measurements of various thicknesses of HOPG. The black open square represents bulk HOPG, while the open diamonds represent HOPG with thicknesses of 2.45 nm (red) and 7.7 nm (blue). Thin graphite ribbons with thicknesses of 8.5 μm , 240 μm , and 580 μm (open circle with a vertical line) were measured using a thermocouple method. (b) Thickness dependence of peak temperature of the measured graphite ribbons compared with various thicknesses of HOPG (2.45 nm, 7.7 nm, 8.5 μm , 240 μm , 580 μm), and 1 mm bulk HOPG. The symbols are the same as for figure (a).

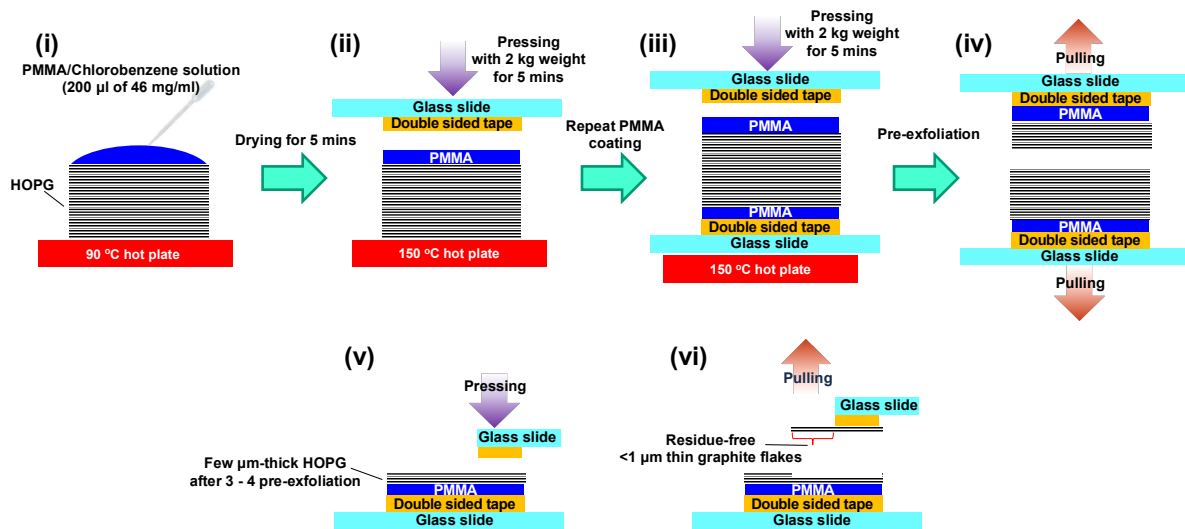
Supplementary information

Thermal transport of suspended thin graphite with unexplored thickness range

Jeon et al.

S1: Thin graphite ribbon preparation

The method used to obtain thin graphite ribbons is described as follows. Highly oriented pyrolytic graphite (HOPG) of ZYA grade from SPI supplies, measuring $12 \times 12 \text{ mm}^2$ and 2 mm thick was used as the starting material. The pre-exfoliation process began by coating the top surface of HOPG with a polymethylmethacrylate (PMMA)/Chlorobenzene solution (46 mg/ml, 200 μl) and drying it at 90 °C for 10 min (Figure S1-i) to facilitate large area exfoliation. Next, the PMMA-coated surface was attached to a double-sided tape/glass slide (Figure S1-ii), and the same process was repeated on the other side. The HOPG sandwiched by double-sided tape/glass slides was then pressed using a 2 kg scientific weight at 150 °C for 5 min (Figure S1-iii). After cooling down to room temperature, the HOPG was exfoliated by pulling the glass slides from both sides (Figure S1-iv). This process was repeated 3 to 4 times to obtain a large area ($12 \times 12 \text{ mm}^2$) and a few micrometer-thick graphite. Finally, the tape residue-free graphite flakes thinner than 1 μm were obtained by attaching and detaching the double-sided tape/glass slide on a small portion of the cleaved HOPG surface (Figure S1-v and vi). The exfoliated thin graphite flakes were then transferred to a metal substrate, covered with a shadow mask, and subjected to O_2 plasma treatment (300 W) for 15 min to obtain thin graphite (TG) ribbons. The thickness of the TG was determined using a surface profilometer (Bruker DektakXT).



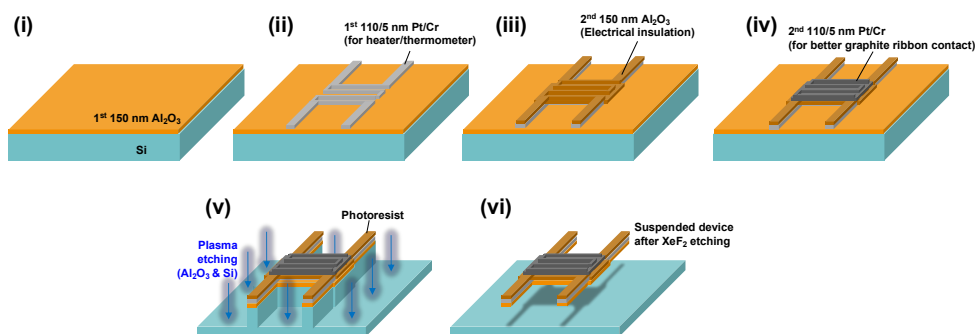
Supplementary Figure S1. Thin graphite ribbon preparation procedure through mechanical exfoliation of bulk HOPG.

S2: Device fabrication and graphite ribbon transfer

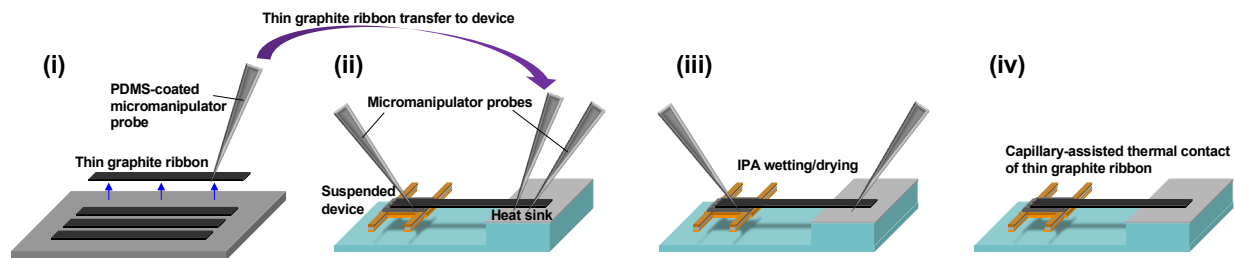
To measure the thermal conductivity of TG, we fabricated suspended electro/thermal microdevices. First, we prepared a 150-nm Al_2O_3 film on a Si wafer (Figure S2-i). Next, we used photolithography to pattern electrodes including a heater/thermometer, beams and wire bonding pads, and heat sink were on top of the Al_2O_3 layer. Then a Pt/Cr (110/5 nm) was deposited by sputtering and the lift-off was carried out using a resist remover (RR41, Futurrex Inc.) (Figure S2-ii). An additional 150-nm Al_2O_3 film was deposited only on the heater/thermometer for electrical insulation between the TG ribbon and electrodes (Figure S2-iii). We also deposited an additional Pt/Cr (110/5 nm) film on the top Al_2O_3 insulation layer to not only reduce the thermal contact resistance by increasing the surface energy with graphite/metal contact,^{1, 2} but also to obtain a uniform temperature profile on the membrane (Figure S2-iv). Except for the patterned area, we dry etched the Al_2O_3 layer using CHF_3 , Cl_2 , and Ar gas (Oxford Plasmalab P80), followed by Si deep reactive ion etching (DRIE) by SF_6 gas (Oxford Plasmalab P100 RIE/ICP) (Figure S2-v). Finally, the heater/thermometer membrane was suspended by removing the Si substrate underneath using XeF_2 etching (Figure S2-vi).

Following the procedure detailed in Supplementary Note S1, TG flakes were obtained and subsequently etched using O_2 plasma treatment (300 W) for 15 min with the aid of a shadow mask, resulting in the formation of TG ribbons (Figure S3-i). Prior to transferring the TG ribbon to the device, the device surface was subjected to a 5 mins oxygen plasma treatment to increase the surface energy by forming a very thin metal oxide layer on Pt and to reduce the Pt roughness for better contact between the TG and the device.^{2, 3} The TG ribbon was then transferred to the device using a micromanipulator with a PDMS-coated probe, with both ends of the TG gently pressed by the other micromanipulators without PDMS to hold it (Figure S3-ii). A small volume of IPA was

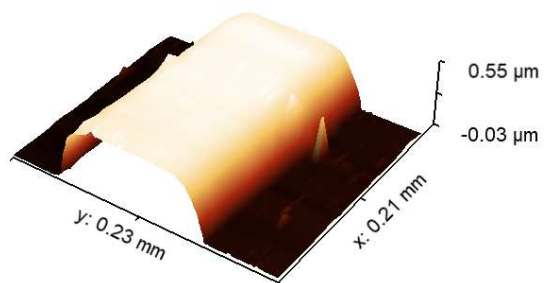
dropped and dried for capillary-assisted thermal contact, which minimizes the thermal contact resistance (Figure S3-iii).^{4, 5} Finally, the suspended graphite ribbon device was obtained (Figure S3-iv).



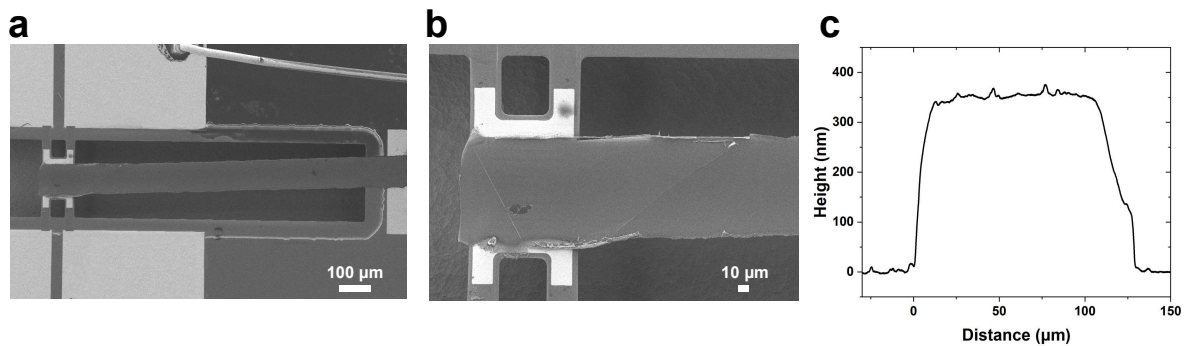
Supplementary Figure S2. Schematics of suspended electrothermal device fabrication procedure.



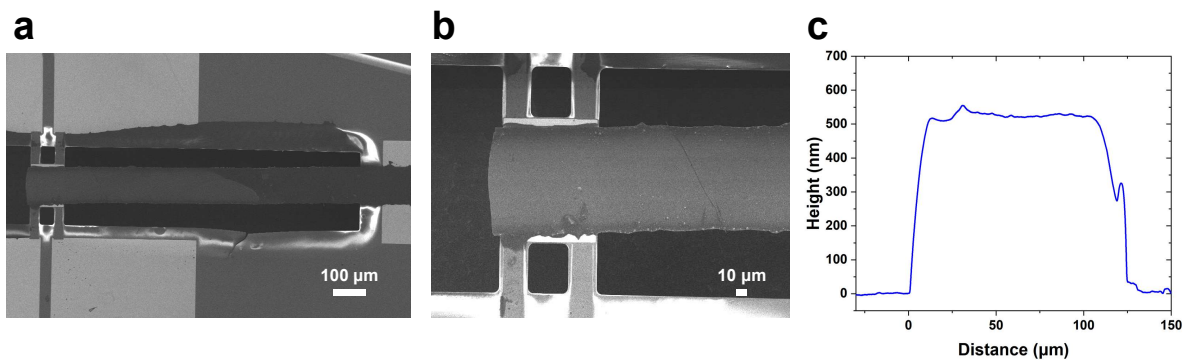
Supplementary Figure S3. Schematics of thin graphite ribbon transfer process to suspended electrothermal device



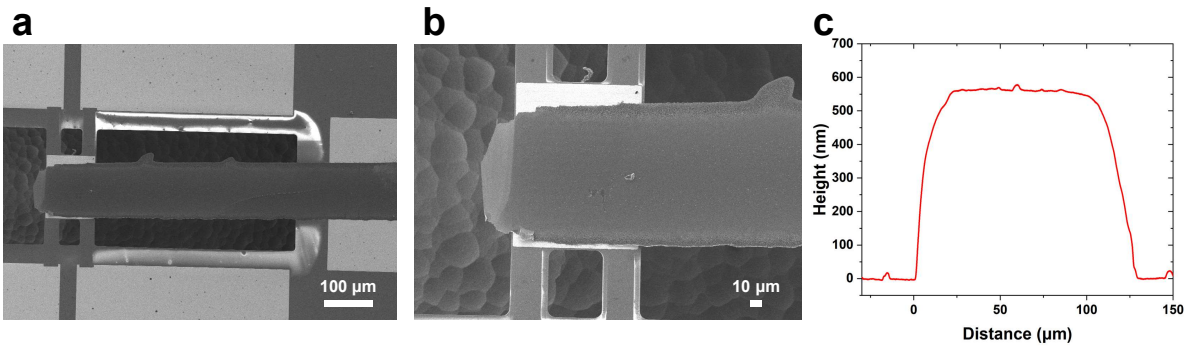
Supplementary Figure S4. 3D map of measured surface profile of ~560 nm thick graphite ribbon (Sample ID: TG3)



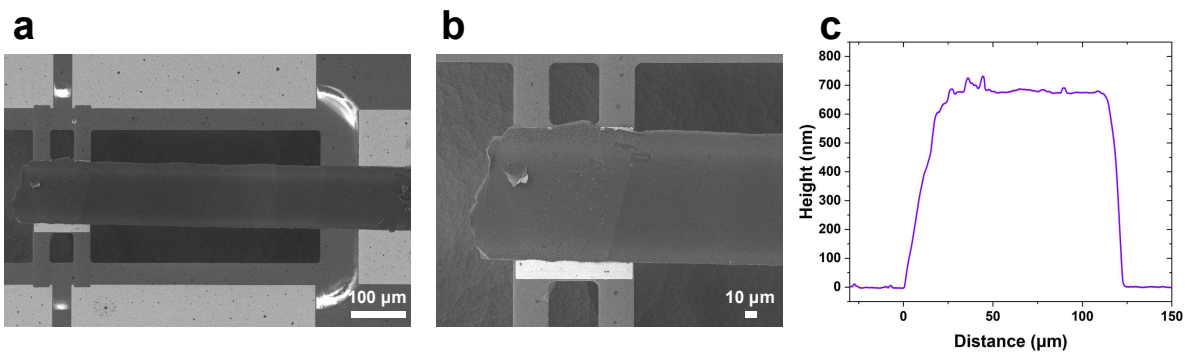
Supplementary Figure S5. SEM images and surface profile of measured ~ 352 nm thick thin graphite ribbon (sample ID: TG1): (a) graphite ribbon length and width from low magnification SEM, (b) contact and alignment of graphite ribbon to suspended heater/thermometer from high magnification SEM, and (c) thickness from a surface profile. Specific geometric for each sample can be found listed in Table 1.



Supplementary Figure S6. SEM images and surface profile of measured ~ 525 nm thick thin graphite ribbon (sample ID: TG2): (a) graphite ribbon length and width from low magnification SEM, (b) contact and alignment of graphite ribbon to suspended heater/thermometer from high magnification SEM, and (c) thickness from a surface profile. Specific geometric for each sample can be found listed in Table 1.



Supplementary Figure S7. SEM images and surface profile of measured ~ 560 nm thick thin graphite ribbon (sample ID: TG3): (a) graphite ribbon length and width from low magnification SEM, (b) contact and alignment of graphite ribbon to suspended heater/thermometer from high magnification SEM, and (c) thickness from a surface profile. Specific geometric for each sample can be found listed in Table 1.



Supplementary Figure S8. SEM images and surface profile of measured ~ 680 nm thick thin graphite ribbon (sample ID: TG4): (a) graphite ribbon length and width from low magnification SEM, (b) contact and alignment of graphite ribbon to suspended heater/thermometer from high magnification SEM, and (c) thickness from a surface profile. Specific geometric for each sample can be found listed in Table 1.

S3: Uncertainty analysis

The error bars of the TG thermal conductivity (κ) in figures 2a and 2b, and figure 3a originate from the combined uncertainties from multiple measurements of thermal conductance of TG (G_{TG}) and dimensions of TG.⁶⁻⁸ The uncertainty of G_{TG} ($u(G_{TG})$) is calculated by Equations S1-S3.⁹

$$G_{TG} = G_t - G_b \quad (S1)$$

$$u(G_{TG}) = \sqrt{\left(\frac{\partial G_{TG}}{\partial G_t}\right)^2 u^2(G_t) + \left(\frac{\partial G_{TG}}{\partial G_b}\right)^2 u^2(G_b)} \quad (S2)$$

$$u(G_{TG}) = \sqrt{u^2(G_t) + u^2(G_b)} \quad (S3)$$

where $G_t (= \frac{Q_t}{\Delta T_h})$ is the combination of thermal conductance of TG and beams (G_b), where the generated heat from the heating membrane ($Q_t = Q_{TG} + Q_b$) conducts through the TG (Q_{TG}) and beams (Q_b). For the reference sample without the graphite ribbon, the heat conducts only through the beams, and therefore $G_b (= \frac{Q_b}{\Delta T_{h,ref}})$ can be obtained by measuring the temperature rise of the heating membrane of the reference sample, $\Delta T_{h,ref}$. The uncertainties $u(G_t)$ and $u(G_b)$ can be calculated using the linear regression from power to temperature rise as shown in Figure S9, which shows clear linear trend indicating very small uncertainties.

Finally, the uncertainty of κ ($u(\kappa)$) is determined by following Equations S4-S6.

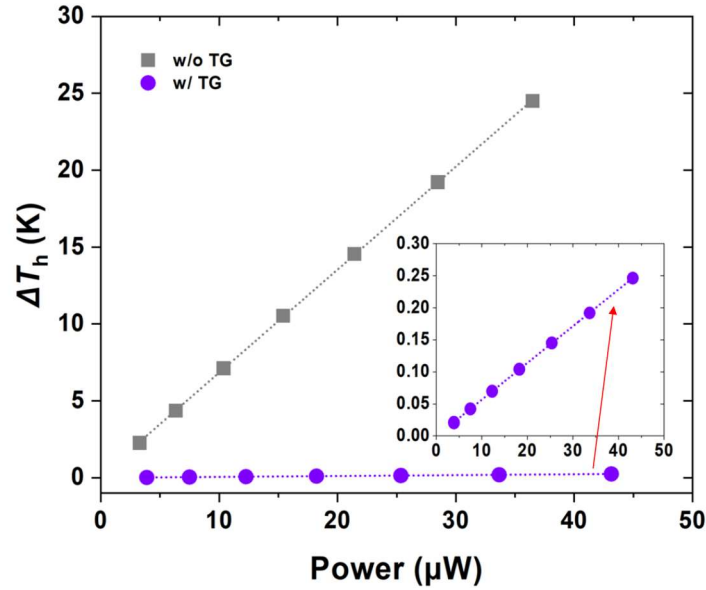
$$\kappa = \frac{G_{TG} \cdot L_{TG}}{A_{TG}} \quad (S4)$$

$$u(\kappa) = \sqrt{\left(\frac{\partial \kappa}{\partial G_{TG}}\right)^2 u^2(G_{TG}) + \left(\frac{\partial \kappa}{\partial L_{TG}}\right)^2 u^2(L_{TG}) + \left(\frac{\partial \kappa}{\partial A_{TG}}\right)^2 u^2(A_{TG})} \quad (S5)$$

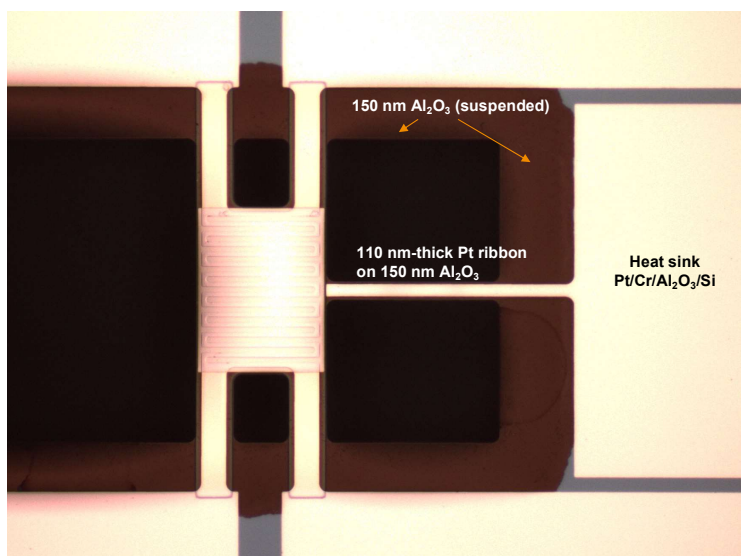
$$u(\kappa) = \sqrt{\left(\frac{L_{TG}}{A_{TG}}\right)^2 u^2(G_{TG}) + \left(\frac{G_{TG}}{A_{TG}}\right)^2 u^2(L_{TG}) + \left(-\frac{G_{TG} \cdot L_{TG}}{A_{TG}^2}\right)^2 u^2(A_{TG})} \quad (S6)$$

where L_{TG} and A_{TG} are the length and the cross-sectional area of the suspended TG ribbon,

respectively. The uncertainties $u(L_{TG})$ and $u(A_{TG})$ are determined from the standard deviations of the width and length measurements from the SEM images and the thickness measurement from the surface profile. Based on these measurements, the value obtained for $u(\kappa)$ was found to be less than 4% in this study.



Supplementary Figure S9. Measured temperature rise on the heating membrane with and without a thin graphite ribbon as a function of heating power. The inset shows the data with the y -axis rescaled to highlight the linear trend of the temperature rise with the thin graphite ribbon. The data are from the 680 nm thick graphite ribbon (sample ID: TG4) measured at 50 K as an example.



Supplementary Figure S10. Optical image of suspended Pt ribbon device. Pt ribbon's thermal conductivity is measured to verify the reliability of our measurement system.

REFERENCES

- (1) Blonski, S.; Garofalini, S. H. Molecular dynamics simulations of α -alumina and γ -alumina surfaces. *Surface Science* **1993**, *295* (1), 263-274. DOI: [https://doi.org/10.1016/0039-6028\(93\)90202-U](https://doi.org/10.1016/0039-6028(93)90202-U).
- (2) Vitos, L.; Ruban, A. V.; Skriver, H. L.; Kollár, J. The surface energy of metals. *Surface Science* **1998**, *411* (1), 186-202. DOI: [https://doi.org/10.1016/S0039-6028\(98\)00363-X](https://doi.org/10.1016/S0039-6028(98)00363-X).
- (3) Li, Z.; Beck, P.; Ohlberg, D. A. A.; Stewart, D. R.; Williams, R. S. Surface properties of platinum thin films as a function of plasma treatment conditions. *Surface Science* **2003**, *529* (3), 410-418. DOI: [https://doi.org/10.1016/S0039-6028\(03\)00015-3](https://doi.org/10.1016/S0039-6028(03)00015-3).
- (4) Shin, S.; Chen, R. Thermal transport measurements of nanostructures using suspended micro-devices. In *Nanoscale Energy Transport*; IOP Publishing, 2020; pp 12-11-12-33. DOI: 10.1088/978-0-7503-1738-2ch12.
- (5) Kim, J.; Seo, D.-J.; Park, H.; Kim, H.; Choi, H.-J.; Kim, W. Extension of the T-bridge method for measuring the thermal conductivity of two-dimensional materials. *Review of Scientific Instruments* **2017**, *88* (5), 054902.
- (6) Shin, S.; Elzouka, M.; Prasher, R.; Chen, R. Far-field coherent thermal emission from polaritonic resonance in individual anisotropic nanoribbons. *Nature communications* **2019**, *10* (1), 1377. DOI: 10.1038/s41467-019-09378-5.
- (7) Shin, S. M.; Chen, R. K. Plasmonically Enhanced Thermal Radiation by Means of Surface Phonon Polaritons. *Phys Rev Appl* **2020**, *14* (6). DOI: ARTN 064013

10.1103/PhysRevApplied.14.064013.

(8) Wingert, M. C.; Chen, Z. C. Y.; Dechaumphai, E.; Moon, J.; Kim, J.-H.; Xiang, J.; Chen, R. Thermal Conductivity of Ge and Ge–Si Core–Shell Nanowires in the Phonon Confinement Regime. *Nano letters* **2011**, *11* (12), 5507-5513. DOI: 10.1021/nl203356h.

(9) Može, M.; Zupančič, M.; Golobič, I. Investigation of the scatter in reported pool boiling CHF measurements including analysis of heat flux and measurement uncertainty evaluation methodology. *Appl Therm Eng* **2020**, *169*, 114938.